Spin dynamics in ferromagnets: Gilbert damping and two-magnon scattering

Kh. Zakeri,* J. Lindner, I. Barsukov, R. Meckenstock, M. Farle, U. von Hörsten, H. Wende, and W. Keune
Fachbereich Physik and Center for Nanointegration (CeNIDE), Universität Duisburg-Essen, Lotharstrasse 1, 47048 Duisburg, Germany

J. Rocker, S. S. Kalarickal,† K. Lenz, W. Kuch, and K. Baberschke
Institut für Experimentalphysik, Freie Universität Berlin, Arnimallee 14, 14195 Berlin, Germany

Z. Frait
Institute of Physics, Academy of Science of the Czech Republic, Na Slovance, 18221 Prague 8, Czech Republic
(Received 10 July 2007; revised manuscript received 10 August 2007; published 14 September 2007)

The magnetic relaxation processes following the dynamical excitation of the spin system of ferromagnets are investigated by ferromagnetic resonance (FMR) between 1 and 70 GHz using epitaxial Fe_3Si films as a prototype system. Two relaxation channels, i.e., dissipative, isotropic Gilbert damping G as well as anisotropic two-magnon scattering Γ, are simultaneously identified by frequency and angle dependent FMR and quantitatively analyzed. The scattering rates due to two-magnon scattering at crystallographic defects for spin waves propagating in $\langle 100\rangle$ and $\langle 110\rangle$ directions, $\gamma\Gamma_{\langle 100\rangle}=0.25(2)$ GHz and $\gamma\Gamma_{\langle 110\rangle}=0.04(2)$ GHz, and the Gilbert damping term $G=0.051(1)$ GHz are determined. We show that changing the film thickness from 8 to 40 nm and slightly modifying the Fe concentration influence the relaxation channels. Our results, which reveal the contributions of longitudinal and transverse relaxation processes may be of general importance for the understanding of spin-wave dynamics in magnetic structures.

DOI: 10.1103/PhysRevB.76.104416 PACS number(s): 76.60.Es, 71.36.+c, 75.50.Bb, 76.50.+g

I. INTRODUCTION

Understanding the magnetic relaxation processes in nanoscale devices has become one of the most interesting challenges in magnetism to date. Linear and nonlinear[1] processes have to be involved to understand new effects such as the vortex core-driven magnetization dynamics,[2] gyroscopic vortex reversal,[3] and ultrafast magnetization reversals by magnetic field pulses or by torque transfer from spin-polarized currents.[4–7] The relaxation of the excited magnetic state involves the dissipation of magnetic energy into spin-wave states, a process which microscopically has not been fully understood since it involves the scattering at defects and longitudinal and transverse relaxation mechanisms. While most experimental studies analyze the overall dynamic response in the framework of the Landau-Lifshitz-Gilbert equation[8] using one phenomenological parameter only, few experimental studies[9–14] have addressed the microscopic origin by trying to distinguish different relaxation channels, which either keep the transverse or the longitudinal component of the magnetization constant. In general, magnetic damping can be split into two fundamentally different channels: (i) Gilbert type relaxation, for which the energy is directly transferred to the lattice, and (ii) non-Gilbert-type damping, which leaves the energy in the spin subsystem by scattering into magnons with nonzero wave vector ($k\neq 0$) and is analogous to a dephasing of the spin precession (transverse relaxation).

This study gives a detailed and quantitative explanation of the damping processes within thin Fe_3Si films grown epitaxially on MgO(001). The Heusler-like alloy Fe_3Si may be an interesting material for *spintronic* devices[15,16] and it can also be viewed as a prototype system for the investigation of relaxation mechanisms due to its narrow ferromagnetic resonance (FMR) linewidth. The results of extensive frequency-dependent (in the range of 1–70 GHz) as well as angle dependent measurements of the FMR linewidth are presented. Fe_3Si is ordered in the cubic $D0_3$ structure [see Fig. 1(a)]. The narrow FMR linewidth leads to a precise determination of the magnetic relaxation parameters of these samples. The benefit of the epitaxial Fe_3Si is that one can distinguish different contributions to the FMR linewidth due to Gilbert damping and other relaxation terms. We present a general model to explain the experimental results of *both* the angular and frequency dependencies of the FMR linewidth yielding a unique set of relaxation parameters. Moreover, we will show that the relative strength of the relaxation parameters can be tuned by changing the film thickness and also by slightly modifying the Fe content.

II. THEORETICAL BACKGROUND

The motion of the sample magnetization $\vec{M}$ in an FMR experiment can be described by

$$\frac{1}{\gamma}\frac{\partial\vec{M}}{\partial t}=-(\vec{M}\times\vec{B}_{\mathrm{eff}})+\vec{R}, \tag{1}$$

where $\vec{B}_{\mathrm{eff}}$ is the effective field, which consists of external as well as internal fields, and γ is the gyromagnetic ratio given by $g\mu_B/\hbar$. Considering only the first term in Eq. (1), one can easily derive the resonance condition[17]

$$\left(\frac{\omega}{\gamma}\right)^2=\frac{1}{M^2\sin^2(\theta)}\left[\frac{\partial^2F}{\partial\theta^2}\frac{\partial^2F}{\partial\phi^2}-\left(\frac{\partial^2F}{\partial\theta\partial\phi}\right)^2\right]. \tag{2}$$

The partial derivatives are evaluated at the angles θ_{eq} and ϕ_{eq} (the equilibrium angles of the magnetization), which mini-

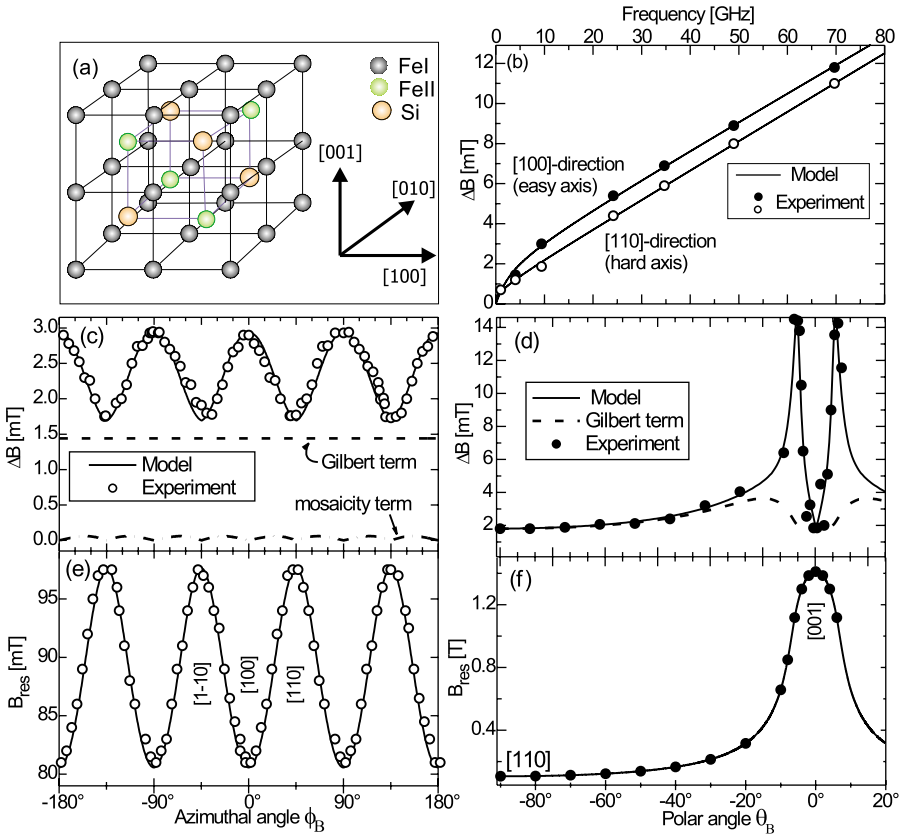

FIG. 1. (Color online) (a) Schematic representation of the $D0_3$ structure of Fe_3Si film. (b) The frequency dependence of the FMR linewidth for an 8 nm Fe_3Si. (c) The azimuthal and (d) the polar angular dependencies of the FMR linewidth measured at a microwave frequency of 9.9 GHz. (e) The azimuthal and (f) the polar angular dependencies of the FMR resonance field measured at the same frequency. All FMR experiments were performed at RT. The error bars are smaller than the symbol size.

mize the free energy F, i.e., $\partial F/\partial\theta=0$ and $\partial F/\partial\phi=0$ (for more details, see Ref. 18).

For a cubic ferromagnetic thin film, the free energy density includes the Zeeman energy, exchange energy, demagnetizing energy, the perpendicular uniaxial $K_{2\perp}$, in-plane uniaxial $K_{2\parallel}$, as well as the cubic K_4 anisotropy energy density,

$$F = -MB[\sin\theta\sin\theta_B\cos(\phi-\phi_B)+\cos\theta\cos\theta_B] - \left(\frac{1}{2}\mu_0M^2 - K_{2\perp}\right)\cos^2\theta + K_{2\parallel}\sin^2\theta\cos^2(\phi-\delta) + K_4\sin^2\theta - \frac{K_4}{8}(7+\cos 4\phi)\sin^4\theta. \quad (3)$$

Here, $\theta_B(\theta)$ and $\phi_B(\phi)$ are the polar and azimuthal angles of the external field $\vec{B}$ (magnetization $\vec{M}$) with respect to the [001] and [100] directions. δ is the angle of the in-plane uniaxial anisotropy with respect to the [100] direction.

This approach is used to determine the anisotropy constants of the system in an FMR experiment.[18] The last term in Eq. (1), $\vec{R}$, represents the precessional damping of $\vec{M}$, which may be written in different phenomenological forms (e.g., Gilbert, Landau-Lifshitz, and Bloch-Bloembergen).[12] It leads to a finite width of the resonance signal within an FMR experiment. However, also the torque term $(\vec{M}\times\vec{B}_{\text{eff}})$ may lead to non-Gilbert type relaxation mechanisms that cannot be included into the conventional damping term. The interplay between Gilbert and non-Gilbert relaxation mechanisms is the focus of the present work and will be discussed in terms of linewidth contributions in the following.

The measured FMR linewidths in this work are analyzed considering four different contributions,

$$\Delta B(\omega,\psi_B) = \Delta B^{\text{Gilbert}}(\omega,\psi_B) + \Delta B^{\text{mosaic}}(\omega,\psi_B) + \Delta B^{\text{2mag}}(\omega,\psi_B) + \Delta B^{\text{inhom}}. \quad (4)$$

Here, ΔB denotes the peak-to-peak linewidth of the FMR signal. ψ_B denotes the two angles θ_B and ϕ_B, the first being the polar angle of the external field measured with respect to the film normal and the second the azimuthal angle of $\vec{B}$ measured with respect to the in-plane [100] direction.

In the following, we briefly describe the four different contributions to the FMR linewidth within Eq. (4).

(i) The Gilbert contribution $\Delta B^{\text{Gilbert}}$. In various magnetic systems, the damping can be described by the phenomenological Gilbert damping parameter G.[8] Sometimes, the dimensionless parameter α is given instead, which is related to G according to $\alpha=G/(\gamma\mu_0M)$. If the Gilbert damping represents the entire intrinsic damping, then it follows from the Landau-Lifshitz-Gilbert equation of motion[8] that the FMR linewidth would depend linearly on the microwave frequency.[12] In order to determine G or α, frequency-dependent FMR measurements over a large range of microwave frequencies are needed. Note that the linear frequency dependence of FMR linewidth is valid *only* when the magnetization and external magnetic field are parallel to each other. Otherwise, the so-called field-dragging contribution

has to be included. If one wants to express relaxation rates in terms of linewidths, i.e., to convert from frequency-swept to the field-swept linewidth measured by FMR, one can use the following conversion (see, for example, Refs. 12 and 19 and references therein):

$$\Delta B(\omega,\psi_B) = \gamma \left| \frac{dB_{\mathrm{res}}(\omega,\psi_B)}{d\omega} \right| \Delta\left(\frac{\omega}{\gamma}\right). \tag{5}$$

Here, $\Delta(\frac{\omega}{\gamma})$ is the frequency-swept linewidth written in magnetic field units. The suffix "res" indicates that $dB_{\mathrm{res}}(\omega,\psi_B)/d\omega$ has to be calculated at the resonance condition. At resonance, ψ_B within Eq. (5) may depend on ω. This is the case when a spatial distribution of the resonance condition and, consequently, of the resonance frequency (or, equivalently, resonance field) is present within the sample and is usually termed (magnetic) mosaicity. In general, Eq. (5) has thus to be written as

$$\Delta B(\omega,\psi_B) = \gamma \left| \frac{\partial B_{\mathrm{res}}(\omega,\psi_B \equiv \mathrm{const})}{\partial\omega} \right| \Delta\left(\frac{\omega}{\gamma}\right) + \gamma \left| \frac{\partial B_{\mathrm{res}}(\omega \equiv \mathrm{const},\psi_B)}{\partial\psi_B} \frac{d\psi_B}{d\omega} \right| \Delta\left(\frac{\omega}{\gamma}\right). \tag{6}$$

The first term in Eq. (6) is commonly called the field-dragging contribution because the partial derivative gets large at angles for which the magnetization $\vec{M}$ is dragged behind $\vec{B}$ due to magnetic anisotropy effects. The second term in Eq. (6) is commonly called the mosaicity contribution. From a standard analysis of the torque equation, the first term in Eq. (6) is the Gilbert damping contribution in Eq. (4) and can be written as[20]

$$\Delta B^{\mathrm{Gilbert}}(\omega,\psi_B \equiv \beta) \approx \frac{2}{\sqrt{3}} \frac{\alpha}{\gamma} \frac{\omega}{\cos\beta}, \tag{7}$$

where β is the angle between the magnetization $\vec{M}$ and external field $\vec{B}$. For the in-plane configuration, $\beta = \phi_{eq} - \phi_B$, and for the out-of-plane configuration, $\beta = \theta_{eq} - \theta_B$. Field dragging ($\cos\beta$ term) in general enhances the damping and only along the hard and easy axes of magnetization, for which $\vec{M}$ and $\vec{B}$ are parallel, the dragging contribution vanishes.

(ii) Line broadening due to mosaicity ($\Delta B^{\mathrm{mosaic}}$) [second term in Eq. (6)]. This term is caused by a small spread of sample parameters on a very large scale.[21] This variation can be found in the internal fields, thickness, or orientation of crystallites within the sample. The individual regions thus have slightly different resonance fields. The overall signal will be a superposition of these local FMR lines yielding a broader linewidth. We consider fluctuations of the *directions* of the anisotropy fields by the mosaicity contribution given by[21]

$$\Delta B^{\mathrm{mosaic}}(\omega,\psi_B) = \left| \frac{\partial B_{\mathrm{res}}(\omega,\psi_B)}{\partial\phi_B} \Delta\phi_B \right| + \left| \frac{\partial B_{\mathrm{res}}(\omega,\psi_B)}{\partial\theta_B} \Delta\theta_B \right|, \tag{8}$$

where $\Delta\phi_B = d\phi_B/d\omega$ and $\Delta\theta_B = d\theta_B/d\omega$ represent the average spread of the direction of the easy axes in the film plane and normal to the film, respectively. Note that for frequency dependent measurements along the easy and hard axes, the partial derivatives are zero and thus the mosaicity contribution vanishes.

There are, however, mechanisms, which cannot be written in Gilbert-like form.[12]

(iii) The two-magnon scattering contribution ΔB^{2mag}. The two-magnon scattering is a process where the $k=0$ magnon excited by FMR scatters into degenerate states of magnons having wave vectors $k \neq 0$.[19] This process requires that the spin-wave dispersion allows for degenerate states, and that there are scattering centers in the sample. The geometrical separation of the scattering centers is connected to the extension of the final magnon states in real space. If long wavelength spin waves are involved in the relaxation process, defects of the order of several hundreds of nanometers rather than atomic defects act as scattering centers. The existence of two-magnon scattering has been demonstrated in many systems of ferrites (see Refs. 9, 22, and 23 and references therein). While in bulk materials this is well known, it was only recently found by several groups to be of major importance also in superlattices[13,14] and ultrathin ferromagnets.[21,24,25]

The linewidth ΔB^{2mag} caused by the two-magnon scattering mechanism is a measure of the scattering rate of the uniform ($k=0$) precession magnons into other spin-wave modes ($k \neq 0$).[9,13,14,26,27] For a homogeneously magnetized thin film, ΔB^{2mag} can be expressed as[28–30]

$$\Delta B^{\mathrm{2mag}}(\omega,\psi_B) = \sum_{\langle x_i \rangle} \Gamma_{\langle x_i \rangle} f(\phi_B - \phi_{\langle x_i \rangle}) \times \arcsin\left[\sqrt{\frac{\sqrt{\omega^2 + (\omega_0/2)^2} - \omega_0/2}{\sqrt{\omega^2 + (\omega_0/2)^2} + \omega_0/2}} \right] \times U(\theta_{eq} - \theta_c), \tag{9}$$

with $\omega_0 = \gamma\mu_0 M_{\mathrm{eff}} = \gamma(\mu_0 M - 2K_{2\perp}/M)$ and $\mu_0 M_{\mathrm{eff}}$ being the effective magnetization that consists of $\mu_0 M$ and the intrinsic out-of-plane anisotropy field $2K_{2\perp}/M$. $\mu_0 M_{\mathrm{eff}}$ can be determined by analyzing the angle dependent FMR resonance field according to Eq. (2). The factor $\Gamma_{\langle x_i \rangle}$ denotes the strength of the two-magnon scattering along the principal in-plane crystallographic direction $\langle x_i \rangle$. This parameter will be fitted to the experimental data. It should be noted that in Refs. 28–30 only the frequency-dependent part of the FMR linewidth was derived [$\Gamma \arcsin(\cdots)$ term in Eq. (9)]. The additional terms added to this contribution will be explained in the following. The $f(\phi_B - \phi_{\langle x_i \rangle})$ term allows for the two-magnon contribution to depend on the in-plane direction of $\vec{B}$ relative to the principal in-plane crystallographic directions $\langle x_i \rangle$ given by the angles $\phi_{\langle x_i \rangle}$. An angle dependent two-magnon scattering may occur when the scattering centers are

not isotropic within the sample. In the case that the centers are given by lattice defects, the angular dependence should reflect this lattice symmetry. In the case that different contributions of two-magnon scattering along the principal crystallographic directions $\langle x_i \rangle$ occur, one has to sum up these contributions weighted by their angular dependence given by f. The step function $U(\theta_{eq}-\theta_c)$ in Eq. (9) is equal to 1 for $\theta_{eq} > \theta_c$ and zero for $\theta_{eq} < \theta_c$. It is used to describe the "switching off" of the two-magnon scattering at a critical out-of-plane angle of the magnetization.[31] Theoretically, it is shown that in oblique configuration, when the magnetization is tipped out of the film plane, finite wave vector modes are degenerate with the FMR mode for $|\theta_{eq}| > |\theta_c| = 45°$. Thus, the two-magnon scattering should be operative in this regime of the tipping angle, but it should shut off for $|\theta_{eq}| < |\theta_c| = 45°$ [see, for example, Eqs. (25)–(27) of Ref. 31]. Such behavior is observed very often in thin metallic ferromagnets.[12,14,25,32] We emphasize that no analytical formula for the angular dependence of the FMR linewidth due to two-magnon scattering has been reported for $|\theta_{eq}| > 45°$ and, thus, for simplification, we neglect the angular dependence of the two-magnon scattering in this regime and approximate the polar angular dependence of the two-magnon scattering by a step function. There are reasons to believe that this indeed is an appropriate approximation. (i) All experimental data reported so far have shown practically no change in the FMR linewidth for $|\theta_{eq}| > 45°$ (see also Refs. 12, 14, 25, and 32), which means that the scattering matrix is rather angle independent. (ii) The overall angular dependence of the FMR linewidth in the out-of-plane configuration for which the static field is varied from the in-plane to the out-of-plane direction is governed by the mosaicity term. Moreover, Ref. 10 shows that the angular dependence due to two-magnon scattering for most cases should lead to a reduction of the linewidth with respect to the in-plane value. This is, however, not observed in the experiment due to the larger dragging and mosaicity contribution. Therefore, the angular dependence caused by two-magnon scattering can be neglected for $|\theta_{eq}| > 45°$. The few studies that experimentally evidence two-magnon scattering in ferromagnets base their conclusion either on the *frequency dependence* of the linewidth being not linear[13,14] or on the *angular dependence* of ΔB at fixed frequency alone.[14,21,24,25]

Although for our films fluctuations of the thickness and thus fluctuations of the *strength* of the anisotropy fields are small, we add a frequency and angle independent broadening term ΔB^{inhom} to Eq. (4) to account for them.[12] ΔB^{inhom} added to the model represents a frequency and angle independent broadening, which cannot be written in the other forms (Gilbert or two-magnon scattering term). As we will show, this contribution plays a minor role in our samples.

III. EXPERIMENTAL DETAILS

8 and 40 nm thick alloy films of nominal composition Fe_3Si and an 8 nm thick alloy film of nominal composition $Fe_{80}Si_{20}$ were grown by molecular beam epitaxy on MgO(001) by codeposition of the isotope ^{57}Fe and Si at a substrate temperature of $T_S = 480$ K with a growth rate of about 1 nm/min, as monitored by a calibrated quartz crystal microbalance. The 8 nm films were annealed *in situ* under ultrahigh vacuum ($p \sim 1 \times 10^{-9}$ mbar) at $T_{ann} = 900$ K for 1 h. After cooling to room temperature, the films were capped with 5 nm of Cr for protection. Thickness and structure of all samples were studied by *ex situ* x-ray diffraction (XRD). The thicknesses given above have been obtained from total thickness oscillations in small-angle XRD. The fundamental (400) reflection of the cubic Fe_3Si structure and the weak (200) superstructure reflection of the $B2$ structure have been observed in θ-2θ high-angle XRD scans. The nominal composition and the $D0_3$ and $B2$ chemical order parameters of the films were determined by ^{57}Fe Mössbauer spectroscopy in combination with spectra simulations.[33] For instance, the actual compositions of our three samples were found to be 25% and 28% Si for the 8 and 40 nm thick films (nominally 25% Si) and 19.5% Si for the 8 nm thick film (nominally 20% Si). The actual 28% Si content of the 40 nm thick film was independently confirmed by Auger electron spectroscopy sputter profiling to be 27.7% Si.[33]

In order to precisely determine the spin relaxation parameters, the frequency dependence of the FMR spectra was investigated within a wide range of microwave frequencies between 1 and 70 GHz. Furthermore, the in- and out-of-plane angular dependencies of the FMR linewidth were recorded at microwave frequencies of 9.9 and 24 GHz. In addition, the saturation magnetization of the samples was measured by a superconducting quantum interference device (SQUID). All FMR and SQUID experiments were performed at room temperature (RT). While the static properties of the samples are reported elsewhere,[34] here, we present the results of the dynamic magnetic properties.

IV. RESULTS AND DISCUSSION

The frequency dependence of the FMR linewidth for an 8 nm thick Fe_3Si film measured along two different in-plane directions, [100] and [110], is shown in Fig. 1(b). The two fit curves in Fig. 1(b) were obtained with the help of our model based on Eq. (4) using fixed angles $\theta_B = 90°$ (external field in plane) and $\phi_B = 0°$ or $\phi_B = 45°$ (external field parallel [100] or [110] direction, respectively). The only fitting parameters used for the frequency-dependent FMR linewidth are ΔB^{inhom}, G, and Γ corresponding to a small frequency-independent inhomogeneous contribution, the Gilbert damping, as well as the two-magnon scattering, respectively. The values of $\mu_0 M_{\text{eff}}$ and g factor that were needed for fitting of the linewidth data were determined by analyzing the azimuthal and polar angular dependencies of the FMR resonance field according to Eq. (2). The angular dependencies of the FMR resonance field and the fits are shown in Figs. 1(e) and 1(f). The fit yielded $\mu_0 M_{\text{eff}} = 1.080(1)T$, $K_4/M = 4.5(1)$ mT (cubic anisotropy field), and $g = 2.075(5)$.[34] The SQUID measurements yielded a saturation magnetization of $\mu_0 M = 1.105$ T. The linewidth broadening due to mosaicity [see Eq. (8)] cannot be determined from the frequency dependence of ΔB along principal axes ($\langle 100 \rangle$ and $\langle 110 \rangle$) because then the partial derivatives in Eq. (8) are zero. In Fig. 1(b), one can see that the curvature along the [100] direction

TABLE I. The magnetic relaxation parameters: (a) 8 nm Fe_3Si annealed at 900 K for 1 h, (b) 40 nm Fe_3Si as prepared, (c) 8 nm $Fe_{80}Si_{20}$ annealed at 900 K for 1 h. All samples were measured at ambient temperature.

Sample	ΔB^{inhom} (mT)	G (10^7 Hz)	$\gamma\Gamma_{\langle 100\rangle}$ (10^7 Hz)	$\gamma\Gamma_{\langle 110\rangle}$ (10^7 Hz)	$\Delta\phi_B$ (deg)	$\Delta\theta_B$ (deg)
(a) 8 nm Fe_3Si annealed	0.2(2)	5.1	25(2)	4(2)	0.09	0.05
(b) 40 nm Fe_3Si as prepared	0.9(1)	5.1(1)	53(17)	26(2)	0.3	0.15
(c) 8 nm $Fe_{80}Si_{20}$ annealed	0	5.8	7(2)	2.65(5)	0.2	

is more pronounced than the along the [110] direction. This clearly indicates the presence of two-magnon scattering, as pure Gilbert-like damping would lead to a linear dependence. The fit parameter Γ in Eq. (9) is a factor scaling the curve with respect to the y axis. The precision of the fit parameters can be enhanced significantly when the in- and out-of-plane angular dependencies of the FMR linewidth are fitted using Eq. (4) for a fixed frequency of $f=9.9$ GHz. The azimuthal and polar angular dependencies of the FMR linewidth are shown in Figs. 1(c) and 1(d), respectively. The polar angle dependent measurement is performed by rotating the external field from the [110] toward the [001] direction. Taking only the Gilbert mechanism according to Eq. (7) into account, one obtains the dashed curves. This clearly shows that the Gilbert mechanism alone is not sufficient to describe the relaxation within the films. In particular, the azimuthal angular dependence of the FMR linewidth should have eight maxima due to the field-dragging effect. Note that due to the small value of G, this angular dependence can hardly be seen. In contrast to the expected behavior, the in-plane angular dependence of the FMR linewidth shows just fourfold (four maxima) symmetry [Fig. 1(a)].

This observation can be explained by considering all contributions of Eq. (4) with the fit parameters obtained from the frequency dependence. There are two issues to note. (i) For all angles between the hard and easy directions, i.e., $\langle 100\rangle$ and $\langle 110\rangle$, field-dragging effects [see Eq. (5)] have to be taken into account because then $\vec{M}$ and $\vec{B}$ are not aligned parallel. This is due to the large demagnetizing field, which acts as an anisotropy contribution. That broadening of the resonance line for the out-of-plane angles $-30° < \theta_B < -5°$ and $5° < \theta_B < 30°$ can be observed nicely in the dashed line of Fig. 1(d). In the in-plane angular dependence, field dragging plays a minor role, as depicted by the almost constant dashed line in Fig. 1(c), since the in-plane anisotropy fields are small. (ii) Comparing the frequency dependencies of the linewidth taken along two distinct directions, it is obvious that the two-magnon contribution is angle dependent. In fact, it has the same fourfold symmetry (four maxima) in the film plane as it is observed for the angular dependence of the resonance position. Such a behavior of anisotropic two-magnon scattering was observed earlier for thin metallic ferromagnets,[25,26] superlattices,[14] as well as *half Heusler* alloy films.[32] In some cases, this could be correlated to defect structures (e.g., dislocation lines) being oriented along distinct crystallographic directions, thus leading to an asymmetry which is the same as the one of the crystal lattice. In the $D0_3$ structure, the $\langle 100\rangle$ and $\langle 110\rangle$ directions are inherently different [Fig. 1(a)]. In such a case, the Fourier component of the defects leads to a fourfold angular dependence being proportional to $f(\phi_B - \phi_{\langle x_i\rangle}) = \cos^2[2(\phi_B - \phi_{\langle x_i\rangle})]$ due to an effective channelling of scattered spin waves (for more details, see Ref. 25). This function was also used to fit the in-plane angular dependence. Note that the fitted curves in Figs. 1(b)–1(d) are not least squares fits of the frequency-dependent data but are the result of a fit to Eq. (4) using both the angular and frequency dependencies of the linewidth yielding a unique set of parameters.

The fits reveal a small mosaicity of the sample in the order of 0.05°–0.1° for $\Delta\phi_B$ and $\Delta\theta_B$. In the film plane, the mosaicity term is slightly bigger than along the perpendicular direction ($\Delta\phi_B > \Delta\theta_B$). This implies that the lateral variation of the anisotropy fields in the film plane (either in orientation or strength) is bigger than the one of the effective demagnetizing field along the perpendicular direction.

In summary, the frequency dependence as well as the angular dependencies for the 8 nm Fe_3Si film can be explained by one set of fit parameters that are summarized in Table I(a). The entire angular dependence can be explained by anisotropic two-magnon scattering and mosaicity effects. No angle dependent Gilbert damping parameter needs to be invoked. The measured intrinsic Gilbert parameter is slightly smaller than the bcc Fe-bulk one (6×10^7 Hz).[35] This is due to the fact that the spin-orbit coupling in this structure is slightly smaller than for bulk Fe.[36–38] The two-magnon scattering along the $\langle 100\rangle$ directions is about five times more effective than that along the $\langle 110\rangle$ directions. Its strength is comparable to the intrinsic Gilbert damping contribution, G, but small in comparison with the values measured for FeV superlattices.[13,14] Indeed, earlier works employing Mössbauer spectroscopy[39] has shown that the defects in bulk Fe_3Si are mainly concentrated in α sublattices [being oriented parallel to the $\langle 100\rangle$ directions, see Fig. 1(a)]. This scenario, which was confirmed recently by first principles density functional calculations in combination with statistical mechanics,[40] naturally explains the fact that the two-magnon contribution is stronger along the $\langle 100\rangle$ directions. According to Refs. 39 and 40, the probability of defect formation along the $\langle 100\rangle$ directions is higher than that along the $\langle 110\rangle$ directions. This already confirms that the $\langle 100\rangle$ and $\langle 110\rangle$ directions are not equivalent. Indeed, Refs. 39 and 40 discuss not only point defects but also preferential diffusion channels. The latter are the ones that to our opinion might lead to large scale defects with average separation on the order of excited spin waves (100 nm) within the film. To quantify these defects is not the goal of this manuscript. We rather propose that such defects must be present.

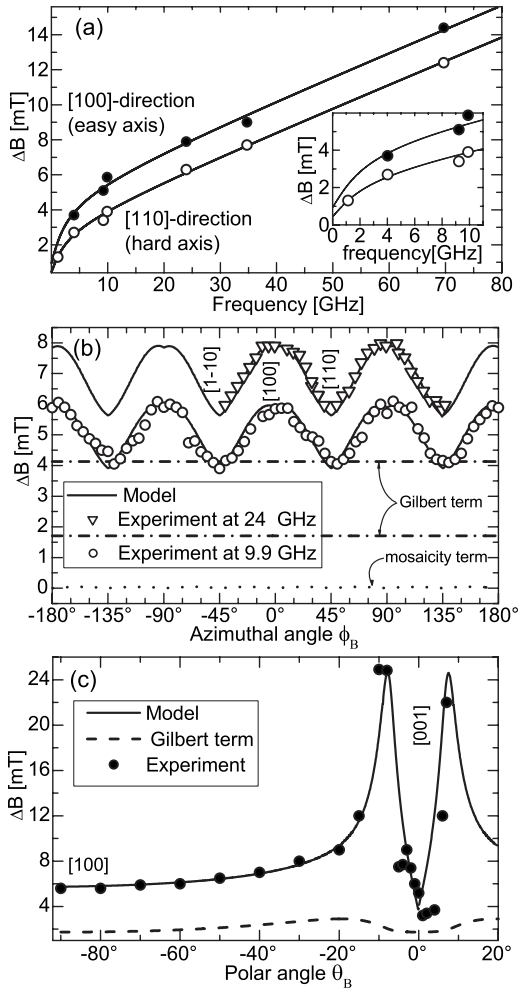

FIG. 2. (a) The frequency dependence of the FMR linewidth for 40 nm Fe_3Si as prepared. The inset shows the low-frequency results. (b) The azimuthal angular dependence of the FMR linewidth measured at microwave frequencies of 9.9 GHz (circles) and 24 GHz (triangles). (c) The polar angular dependence of the FMR linewidth recorded at 9.9 GHz. All experiments were performed at RT. The error bars are smaller than the symbol size.

We point out that there are other broadening mechanisms, i.e., exchange-conductivity, surface pinning, or surface anisotropy effects.[41] To account for their possible contribution, we have performed the calculations using the formulas for FMR microwave absorption obtained from the equation of motion and Maxwell and boundary equations[41] of the linewidth contribution caused by exchange-conductivity and by surface spin pinning effects. For our case, $\mu_0 M_{\text{eff}} \sim 1$ T, $g \sim 2.075$, $G = 5.1 \times 10^7$ Hz, and film thickness of 8–40 nm, both linewidth contributions are less than 0.1 mT for 18–70 GHz. Therefore, they can be neglected.

If lattice defects in the volume of the film and not at the interfaces are the origin of the two-magnon scattering, one would expect that its strength increases with film thickness when the volume part of the film becomes the dominating contribution. This is demonstrated in Fig. 2, where the frequency and angular dependencies of the FMR linewidth of an as-prepared (not annealed) 40 nm thick sample are plotted. The values for this film were obtained in the same way as described for the case of the 8 nm thick sample. They indeed show [see Table I(b)] that the two-magnon contribution is increased along both principal in-plane directions. While the Gilbert contribution is the same (G is a material dependent constant), the two-magnon contribution has even overcome the Gilbert damping along the ⟨100⟩ directions [see Table I(b)].

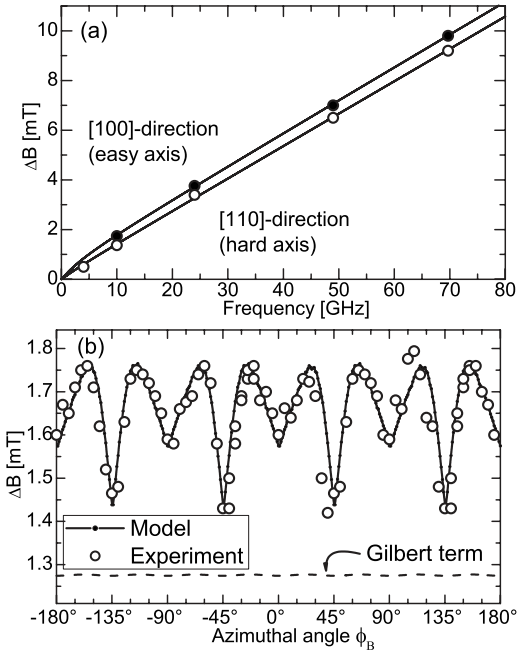

FIG. 3. (a) The frequency dependence of the FMR linewidth for an 8 nm $Fe_{80}Si_{20}$ film annealed at 900 K. (b) The azimuthal angular dependence of the FMR linewidth measured at 9.9 GHz. All experiments were performed at ambient temperature. The error bars are smaller than the symbol size.

One notices that the two-magnon scattering strength for the 40 nm film is about twice that of the 8 nm film. This is mainly due to the change in the available density of states for the degenerate magnons in the thicker film. This thickness dependence has been established recently in Ref. 42. The enhanced two-magnon scattering in the 40 nm sample is another experimental confirmation of the theory that has been recently developed by Krivosik *et al.*[42] The authors showed that the available density of states for the degenerate magnons increase for thicker films. In addition, the larger mosaicity supports the fact that the thicker film has less structural perfection than the 8 nm thick one. We note, however, that the structural imperfection could also be related to the fact that this sample was not annealed. In the thick sample with stronger two-magnon scattering, another effect can be observed in Fig. 2(c): the linewidth along the film normal is smaller than the one in the film plane. The dragging effect as a cause can be ruled out, as $\vec{M}$ and $\vec{B}$ are parallel in these directions (see discussion above) and also the Gilbert contribution is the same. Thus, one has to conclude that the two-magnon scattering depends on the polar angle, being *switched off* for the perpendicular geometry.

It was found experimentally[39] and later theoretically[40] that the defect formation energy increases with increasing Fe

concentration, i.e., less defects are expected for a larger amount of Fe. In order to monitor this effect, an 8 nm $Fe_{80}Si_{20}$ film was prepared. The phase diagram of $Fe_{100-x}Si_x$ shows that the $D0_3$ structure is stable in the Si-concentration range between $12.5\% < x < 31\%$.[43] Therefore, a structural transformation due to the reduction of the Si concentration can be ruled out as it is also demonstrated by our x-ray diffraction experiments.[34]

The frequency and angular dependencies of the 8 nm $Fe_{80}Si_{20}$ film are shown in Fig. 3. It is obvious that the two-magnon scattering contribution is now much smaller than that in the stoichiometric sample (Fig. 1). The in-plane angular dependence of the FMR linewidth in Fig. 3(b) shows eight maxima that is expected from a mosaicity driven linewidth broadening as well as for a strong field-dragging contribution in the Gilbert damping. It can be seen that a smaller fourfold symmetry (four maxima) is superimposed on the eight maxima, indicating that two-magnon scattering is still present. This time, its strength is much smaller than the mosaicity effect.

The magnetic relaxation parameters are listed in Table I(c). The Gilbert parameter G is found to be slightly larger than that in the stoichiometric Fe_3Si film, which means a slightly larger spin-orbit coupling for this structure as expected due to the larger Fe content. We note that this enhancement is also confirmed by measurements of the g factor as well as the magnetic anisotropy, which also show a slight increase with respect to the stoichiometric sample.[34] As both quantities are related to orbital magnetism, they support the finding of a larger Gilbert parameter.

V. CONCLUSION

The magnetic relaxation mechanisms in thin epitaxial Fe_3Si and $Fe_{80}Si_{20}$ films were investigated using FMR in a wide range of microwave frequencies (1–70 GHz). A comprehensive measurement and analysis of two separate and independent observables in the FMR linewidth, namely, the angular and frequency dependencies, is presented. It is shown that the measured physical parameters, Gilbert damping as well as the spin-wave excitation rate $\gamma\Gamma$, allow a complete understanding of the frequency and the angle dependent linewidth data simultaneously.

The model by Arias and Mills[28–30] is confirmed for thin magnetic structures. We showed that the Gilbert damping parameter and the non-Gilbert-type relaxation rates can be tuned by slightly modifying the Fe concentration or film thickness or by annealing. These results are important also from the applications, i.e., the magnetization reversal and dynamic response in *spintronic* devices.

ACKNOWLEDGMENT

This work has been supported by the Deutsche Forschungsgemeinschaft, Sfb 491.

*zakeri@agfarle.uni-duisburg.de

†Present address: Department of Physics, Colorado State University, Fort Collins, CO 80523, USA.

[1] M. Wu, B. A. Kalinikos, L. D. Carr, and C. E. Patton, Phys. Rev. Lett. **96**, 187202 (2006).

[2] S.-B. Choe, Y. Acremann, A. Scholl, A. Bauer, A. Doran, J. Stöhr, and H. A. Padmore, Science **304**, 420 (2004).

[3] B. Van Waeyenberge, A. Puzic, H. Stoll, K. W. Chou, T. Tyliszczak, R. Hertel, M. Fähnle, H. Brückl, K. Rott, G. Reiss, I. Neudecker, D. Weiss, C. H. Back, and G. Schütz, Nature (London) **444**, 461 (2006).

[4] J. A. Katine, F. J. Albert, R. A. Buhrman, E. B. Myers, and D. C. Ralph, Phys. Rev. Lett. **84**, 3149 (2000).

[5] S. Petit, C. Baraduc, C. Thirion, U. Ebels, Y. Liu, M. Li, P. Wang, and B. Dieny, Phys. Rev. Lett. **98**, 077203 (2007).

[6] J. Ho, F. C. Khanna, and B. C. Choi, Phys. Rev. Lett. **92**, 097601 (2004).

[7] S. Zhang, P. M. Levy, and A. Fert, Phys. Rev. Lett. **88**, 236601 (2002).

[8] T. L. Gilbert, IEEE Trans. Magn. **40**, 3443 (2004); Ph.D. thesis, Illinois Institute of Technology, 1956.

[9] M. J. Hurben and C. E. Patton, J. Appl. Phys. **83**, 4344 (1998).

[10] R. D. McMichael and P. Krivosik, IEEE Trans. Magn. **40**, 2 (2004).

[11] B. J. Kuanr, R. E. Camley, and Z. Celinski, J. Appl. Phys. **95**, 6610 (2004).

[12] B. Heinrich, *Ultrathin Magnetic Structures*, Fundamentals of Nanomagnetism Vol. III, edited by J. A. C. Bland and B. Heinrich (Springer, Berlin, 2005).

[13] J. Lindner, K. Lenz, E. Kosubek, K. Baberschke, D. Spoddig, R. Meckenstock, J. Pelzl, Z. Frait, and D. L. Mills, Phys. Rev. B **68**, 060102(R) (2003).

[14] K. Lenz, H. Wende, W. Kuch, K. Baberschke, K. Nagy, and A. Jánossy, Phys. Rev. B **73**, 144424 (2006).

[15] A. Kawaharazuka, M. Ramsteiner, J. Herfort, H. P. Schönherr, H. Kostial, and K. H. Ploog, Appl. Phys. Lett. **85**, 3492 (2004).

[16] S. Adoh, M. Kumano, R. Kizuka, K. Ueda, A. Kenjo, and M. Miyao, Appl. Phys. Lett. **89**, 182511 (2006); R. Nakane, M. Tanaka, S. Sugahara, *ibid.* **89**, 192503 (2006); T. Yoshitake, D. Nakagauchi, T. Ogawa, M. Itakura, N. Kuwano, Y. Tomokiyo, T. Kajiwara, and K. Nagayama, *ibid.* **86**, 262505 (2005).

[17] J. Smit and H. G. Beljers, Philips Res. Rep. **10**, 133 (1955).

[18] M. Farle, Rep. Prog. Phys. **61**, 755 (1998).

[19] M. Sparks, *Ferromagnetic-Relaxation Theory* (McGraw-Hill, New York, 1964).

[20] S. V. Vonsovski, *Ferromagnetic Resonance* (Pergamon, Oxford, 1960).

[21] R. D. McMichael, D. J. Twisselmann, and A. Kunz, Phys. Rev. Lett. **90**, 227601 (2003).

[22] A. V. Nazarov, D. Menard, J. J. Green, C. E. Patton, G. M. Argentina, and H. J. Van Hook, J. Appl. Phys. **94**, 7227 (2003).

[23] N. Mo, Y.-Y. Song, and C. E. Patton, J. Appl. Phys. **97**, 093901 (2005).

[24] A. Butera, J. Gómez, J. L. Weston, and J. A. Barnard, J. Appl.

Phys. **98**, 033901 (2005).
[25] G. Woltersdorf and B. Heinrich, Phys. Rev. B **69**, 184417 (2004).
[26] R. Urban, G. Woltersdorf, and B. Heinrich, Phys. Rev. Lett. **87**, 217204 (2001).
[27] K. Lenz, T. Toliński, J. Lindner, E. Kosubek, and K. Baberschke, Phys. Rev. B **69**, 144422 (2004).
[28] R. Arias and D. L. Mills, Phys. Rev. B **60**, 7395 (1999).
[29] R. Arias and D. L. Mills, J. Appl. Phys. **87**, 5455 (2000).
[30] D. L. Mills and R. Arias, Physica B **384**, 147 (2006).
[31] D. L. Mills and S. M. Rezende, in *Spin Dynamics in Confined Magnetic Structures II*, edited B. Hillebrands and K. Ounadjela (Springer-Verlag, Berlin, 2003), pp. 45–46.
[32] B. Heinrich, G. Woltersdorf, R. Urban, O. Mosendz, G. Schmidt, P. Bach, L. Molenkamp, and E. Rozenberg, J. Appl. Phys. **95**, 7462 (2004).
[33] N. Utochkina, M. Walterfang, U. von Hörsten, W. Keune, H. Wende, and H. Reuther (unpublished).
[34] Kh. Zakeri, I. Barsukov, N. K. Utochkina, F. M. Römer, J. Lindner, R. Meckenstock, U. von Hörsten, H. Wende, W. Keune, M. Farle, S. S. Kalarickal, K. Lenz, and Z. Frait (unpublished).
[35] Z. Frait and D. Fraitova, J. Magn. Magn. Mater. **15-18**, 1081 (1980).
[36] Y. Nakamura, *Alloys and Compounds of d-Elements with Main Group Elements*, Landolt-Börnstein, New Series, Group III, Vol. 19, Part C (Springer, Berlin, 1988), p. 26.
[37] K. Lenz, E. Kosubek, K. Baberschke, H. Wende, J. Herfort, H.-P. Schönherr, and K. H. Ploog, Phys. Rev. B **72**, 144411 (2005); K. Lenz, E. Kosubek, K. Baberschke, J. Herfort, H.-P. Schönherr, and K. H. Ploog, Phys. Status Solidi C **3**, 122 (2006).
[38] A. Ionescu, C. A. F. Vaz, T. Trypiniotis, C. M. Gürtler, H. García-Miquel, J. A. C. Bland, M. E. Vickers, R. M. Dalgliesh, S. Langridge, Y. Bugoslavsky, Y. Miyoshi, L. F. Cohen, and K. R. A. Ziebeck, Phys. Rev. B **71**, 094401 (2005); A. Ionescu, C. A. F. Vaz, T. Trypiniotis, C. M. Gürtler, M. E. Vickers, H. García-Miquel, and J. A. C. Bland, J. Magn. Magn. Mater. **286**, 72 (2005).
[39] B. Sepiol and G. Vogl, Phys. Rev. Lett. **71**, 731 (1993), and references therein.
[40] S. Dennler and J. Hafner, Phys. Rev. B **73**, 174303 (2006).
[41] Z. Frait and H. MacFaden, Phys. Rev. **139**, A1173 (1965).
[42] P. Krivosik, N. Mo, S. Kalarickal, and C. E. Patton, J. Appl. Phys. **101**, 083901 (2007).
[43] T. B. Massalski, *Binary Alloy Phase Diagrams* (American Society for Metals, Metals Park, OH, 1986).